The Effects of Incomplete Breath-Holding on 3D MR Image Quality

Jeffrey H. Maki, MD, PhD • Thomas L. Chenevert, PhD • Martin R. Prince MD, PhD

The purpose of this study was to investigate how fast three-dimensional (3D) MR image quality is affected by breath-holding and to develop an optimal breath-holding strategy that minimizes artifact in the event of an incomplete breath-hold. A computer model was developed to study variable-duration breath-holds during fast 3D imaging. Modeling was validated by 3D gradient-echo imaging performed on 10 volunteers. Signal-to-noise ratio (SNR) and image blur were measured for both simulated and clinical images. Insights gained were applied to clinical 3D gadolinium-enhanced MR angiography. Breath-holding significantly improved abdominal 3D MR image quality. Most of this benefit could be achieved with a breath-hold fraction of 50% if it occurred during acquisition of central k space. Breath-holding during peripheral k-space acquisition, however, had no significant benefit. Respiratory motion artifact on fast 3D MRI occurring when a patient fails to suspend respiration for the entire scan duration can be minimized by collecting central k space first (centric acquisition) so that premature breathing affects only the acquisition of peripheral k space.

Index terms: MRI • Phase-encoding order • Motion correction • MR artifact • MR angiography • 3D imaging

JMRI 1997; 7:1132–1139

Abbreviations: 1D = one-dimensional, 2D = two-dimensional, 3D = three-dimensional, FOV = field of view, Gd = gadolinium, Gd-MRA = gadolinium-enhanced MR angiography, MIP = maximum intensity projection, MRA = MR angiography, ROI = region of interest, SNR = signal-to-noise ratio.

From the University of Michigan, Department of Radiology, Division of MRI, University Hospital Box 0030, Ann Arbor, MI 48109-0030. Received February 6, 1997; revision requested March 31; revision received June 9; accepted July 18. Supported, in part, by a grant from the Whitaker Foundation. This work was presented as a poster at the 1997 meeting of the International Society for Magnetic Resonance in Medicine. **Address reprint requests to** J.H.M.

AS MRI BECOMES increasingly faster, a growing number of examinations can be performed during breath-holding. This is particularly important for fast three-dimensional (3D) gradient-echo applications such as gadolinium-enhanced MR angiography (Gd-MRA). In the abdomen and thorax, breath-holding significantly decreases motion-related artifacts such as blurring and ghosting (1–5). Frequently, however, patients are unable or unwilling to cooperate with breathing instructions completely. Under these circumstances, breath-holding is not always maintained for the full scan duration. We term this "partial" breath-holding, and it leads to a variable degree of image degradation.

In this study (mainly targeting dynamic imaging using fast volume acquisition techniques), we begin with the commonly accepted premise that partial breath-holding is more effective if it occurs during acquisition of the central portion of k space (low spatial frequencies). We then hypothesize that a partial breath-hold period exists for which image degradation is acceptable, thus no longer constraining scan time to the maximal breath-hold duration. Using computer modeling and imaging of normal volunteers, we test this hypothesis by evaluating the degree of image degradation that occurs for different breath-hold fractions.

• METHODS

Computer Modeling

Periodic respiratory motion causes a modulation in the phase-encoding data, which in turn leads to ghosting, blurring, and signal intensity loss (1,6). For two-dimensional (2D) imaging, the ghosting artifacts are most pronounced in the phase-encoding direction (y), but it should also be noted that view-to-view displacement in the readout direction (x) causes readout direction artifacts as well. For 3D imaging, ghosting artifacts mainly occur in both phase-encoding directions (y and z). If the respiratory period is significantly longer than the duration of the fast phase-encoding loop (z), the z direction phase inconsistencies (and hence artifacts) are much less pronounced than those in the y direction and mainly consist of blurring. This is the case for a typical fast 3D sequence (as used in Gd-MRA), in which approximately 32 slices are acquired at a TR of less than 8 msec for a fast encoding duration less than 260 msec. This is indeed short compared with an average respiratory period. By

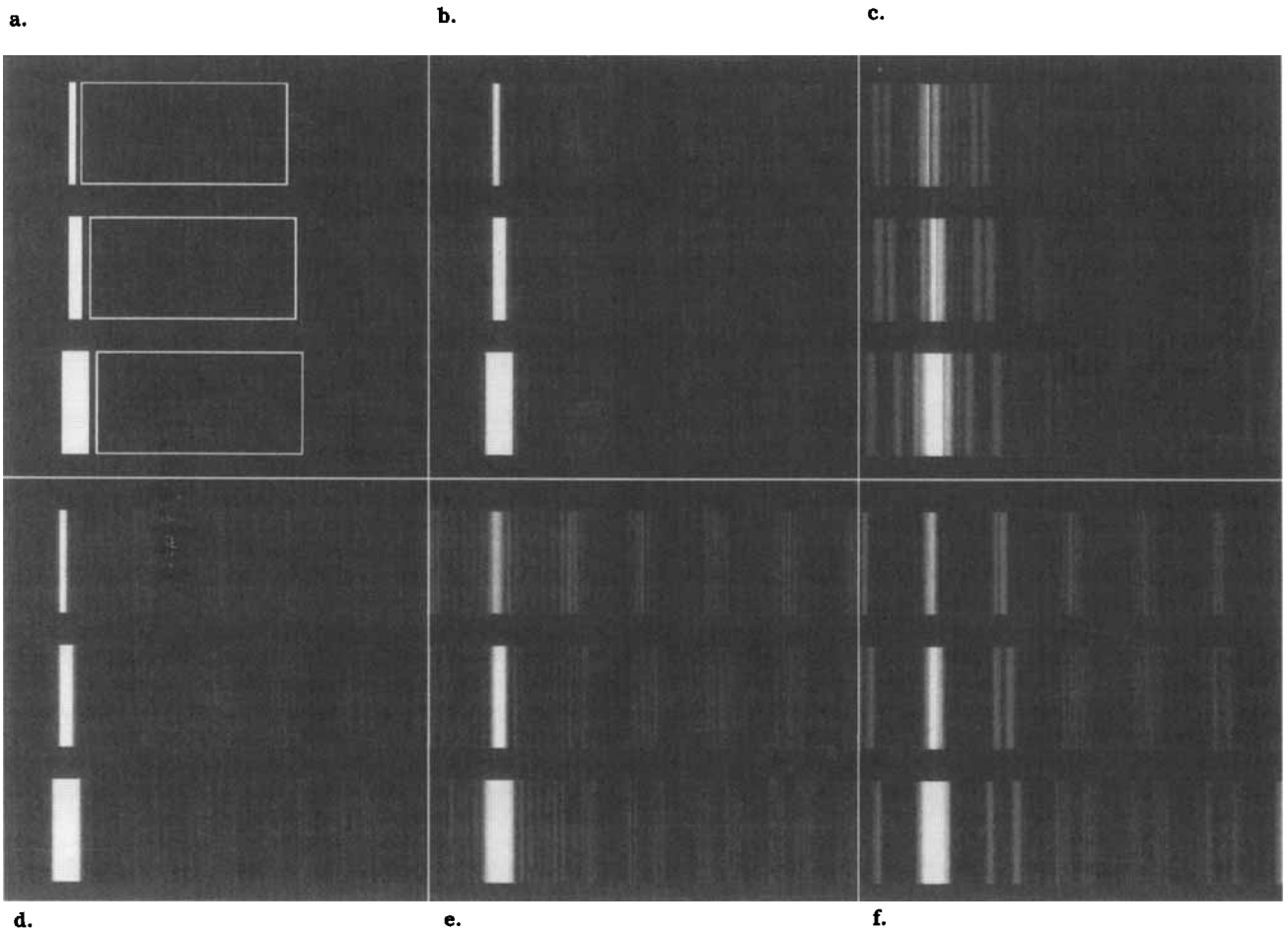

Figure 1. Computer simulation of partial breath-holding for three varying sized "vessels." Partial breath-holds occurred either during central or peripheral k-space acquisition (cyclic respiratory motion in the phase direction [left to right], rate = 18 cycles/min, amplitude = 4 pixels). Breath-hold fraction/position with respect to k-space acquisition: **(a)** 100% breath-hold (air ROIs shown — phantom ROIs encompassed the full corresponding phantom length and width, except for the large phantom, in which ROI width was 83% of phantom width), **(b)** 75% central breath-hold, **(c)** 75% peripheral breath-hold, **(d)** 50% central breath-hold, **(e)** 25% central breath-hold, **(f)** free breathing.

contrast, the slow phase encoding occurs over the entire scan duration, which, in this example, is approximately 33 seconds (for 128 phase encodings).

To evaluate the effects of respiratory motion and breath-holding on image quality, a 2D computer model was developed to simulate the artifacts generated by a fast 3D sequence. In this model, no motion was assumed in the fast encoding direction (z). This simplification is justified, as it is predominately the larger magnitude, slow encoding (y) direction artifacts that are of interest. Because there is no motion in the z (fast encoding) direction, there is no motion-induced phase shift in z, and therefore, the one-dimensional (1D) transform in z is not corrupted, even with motion in x and y. Under these circumstances, the 3D situation can be modeled in two dimensions by scaling the time between successive changes in the slow phase-encoding index (k_y) from TR to TR*ZRES, where ZRES is the number of phase encodings in z. Thus, for a given k_y, the appropriate position-dependent phase shift is applied to each element k_x of the Fourier transform of the "actual" simulated image. As k_y is incremented, a new phase shift based on the position at time TR*ZRES later is applied to each element of k_x, etc. For k_y values in which breath holding is implemented, the phase shift is constant. The sequence used a "centric" acquisition scheme in k_y, whereby the lowest frequency component (center) of k space is obtained first, followed by alternating positive and negative higher and higher spatial frequency components (7,8).

This model was implemented (MATLAB, MathWorks, Inc., Natick, MA) with a simulated 192 × 192 MR angiography (MRA) image that included three "vessels" measuring 3, 6, and 12 pixels in diameter (6.25, 12.5, and 25 mm for a 40-cm field of view [FOV]). Simulated motion (at a rate of 15–21 cycles/min, amplitude 4 pixels, repeating Gaussian waveform to more realistically simulate real breathing, ie, displacement = $4e^{-t^2/2\sigma^2}$ where σ = .5 second) was then added in the phase-encoding (y) direction to simulate respiration. The 4-pixel amplitude was chosen based on the results of the human volunteer studies (see below). Modeled parameters were kept identical to the clinical parameters (TR = 7 msec, 32 slices, 192 phase encodings, one excitation). Breath-hold duration (at full inspiration) was incremented by 5% steps, both at the beginning and the end of a modeled centric acquisition. We hereafter refer to these breath-holds as "central" and "peripheral," reflecting the region of k space over which the breath-hold occurs. Gaussian random noise was added to the simulated k-space data such that the motionless signal-to-noise ratio (SNR) in the reconstructed motionless images was comparable to that of the clinical images (SNR approximately 48). SNR and blur were measured and

then averaged for three simulations at different respiratory rates. Figure 1 demonstrates an example of computer-modeled images.

Human Subjects

Ten healthy volunteers were enrolled in this study over a 1-month period using the informed consent process under the supervision of the Institutional Review Board. Each volunteer was given general instructions in the different breathing regimens (see below) before the study and specific instructions before each image acquisition. A 60-ml syringe (25-mm diameter) filled with a 2.9-mmol solution of gadopentetate dimeglumine (T1 ~ 75 msec) was taped to each subject's abdomen to simulate an enhanced vascular structure undergoing respiratory motion. The subjects consisted of 9 men and 1 woman, ranging in age from 25 to 39 years.

Imaging

All imaging was performed on a 1.5-T imaging system (Horizon, General Electric Medical Systems, Milwaukee, WI). Using the body coil, multiple sagittal 3D fast spoiled gradient-echo sequences were performed through the left aspect of the abdomen (TR = 7 msec, TE = 1.2 msec, flip angle = 30°, 32 slices, 3.5-mm slice thickness, FOV = 36–42 cm, bandwidth = 32 kHz, one excitation, matrix = 256 × 192). Acquisition was "centric," which for our imaging system means centric in the slow phase-encoding (outer loop) direction and sequential in the fast phase-encoding (inner loop) direction. The sequence was run for approximately 4 seconds before collecting actual image data to ensure that equilibrium was reached. Total scan time was 47 seconds.

This sequence was run 15 times on each volunteer in the following order: 1) 100% breath-hold, 2) normal breathing, 3) heavy breathing, 4) 100% breath-hold, 5) 80% central breath-hold, 6) 65% central breath-hold, 7) 50% central breath-hold, 8) 35% central breath-hold, 9) 20% central breath-hold, 10) 75% peripheral breath-hold, 11) 50% peripheral breath-hold, 12) 25% peripheral breath-hold, 13) normal breathing, 14) breath-hold expiration, and 15) 100% breath-hold. The 100% breath-holds and normal breathing were obtained at multiple times to assess consistency and decrease the effects of any inadvertent motion during the breath-holds. Adequate resting time (approximately 30 seconds) was given between runs, and compliance with breathing instructions was closely monitored by a radiologist (J.H.M.) in the scanner room watching both the subject's chest motion and the output from a respiratory bellows system. Breath-hold times were communicated to the subject by means of prearranged shaking of the subject's foot when respiration was to begin or halt. This protocol was not difficult for any of the healthy volunteers. Note that because of the study design, some central and peripheral breath-holds were not of the exact same duration (80% vs 75% and 20% vs 25%). This was performed to increase the number of central breath-hold data points, which we believed was the more important technique. Example images are shown in Figure 2.

Image Analysis

For each subject, different sagittal slice locations were chosen to include cross-sections through the gadolinium (Gd) phantom, the inferior perirenal fat, and the liver. Using region-of-interest (ROI) analysis, the mean signal intensity was measured for each of these structures in each breathing experiment. Similarly, the mean of each of the three simulated tubes was measured. The SNR was then calculated by dividing the mean intensity of each structure by the SD of a relatively large adjacent region of air (same level in the phase direction). Because only noise should be present in air, it is not necessary to correct for a Rician noise distribution, as the Rician and Gaussian distributions differ only by a constant, and we are only concerned with relative SNR (9). SNRs were normalized to a 40-cm FOV ($SNR_{40} = 40^2/FOV^2 * SNR$) and averaged for all 10 subjects.

Line profiles perpendicular to the long axis of the phantom were obtained for both human and simulated images. Partial volume effects were minimized by choosing a sagittal slice centered directly through the phantom and trying to position the phantom on the abdomen with minimal inclination. The degree of blurring was then calculated by evaluating the upslope of the line profile (transition from air to phantom). Blur data are reported as the distance (mm) spanning 20% to 80% of average maximum phantom intensity; the minimum blur was defined as the width of one pixel. Linear interpolation was used to estimate the 20% to 80% transition width.

Contamination, which we define as the change in variance (power) within an ROI due to superimposed respiratory artifacts, was measured in the psoas muscle. Psoas was chosen because it is nearly stationary, and an ROI could be chosen at the same level (in both the slice and phase directions) as the high signal intensity phantom, thus accentuating the "splattered" respiratory artifacts propagating in the phase-encoding direction (see Fig. 2). Using the signal variance (square of the SD) of the breath-hold as a baseline, the increase in variance was measured versus early breath-hold fraction.

Statistical Analysis

Using a paired two-tailed Student *t* test, statistical analysis was performed on the human subject SNR and blur measurements to (*a*) evaluate the statistical significance of the differences between central and peripheral breath-holding, (*b*) determine the statistical significance of partial breath-holding versus free breathing, and (*c*) determine the level of significance in differences between complete and partial breath-holding.

Patient Studies

Examples from three different patients undergoing Gd-MRA are presented. Representative maximum intensity projection (MIP) images were obtained from the arterial phase of fast 3D spoiled gradient-refocused angiograms of the renal arteries for each patient (Figs. 3a through 3c). All patients received a bolus administration of 40 ml of gadopentetate dimeglumine and were asked to suspend respiration at the start of scanning. Data acquisition was centric, with TR = 5.2 to 7.2 msec, TE = 1.2 to 1.3 msec, number slices = 32 to 44, slice thickness = 2.5 mm, and total acquisition time = 28 to 39 seconds. One patient was unable to stop breathing (0% breath-hold) and a second patient was only able to breath-hold for 16 of 28 seconds (57% breath-hold), whereas the final patient completed a full breath-hold (100% breath-hold).

• RESULTS

Computer Modeling

Simulated partial breath-hold images are shown in Figure 1. Respiratory artifact is highly dependent on where

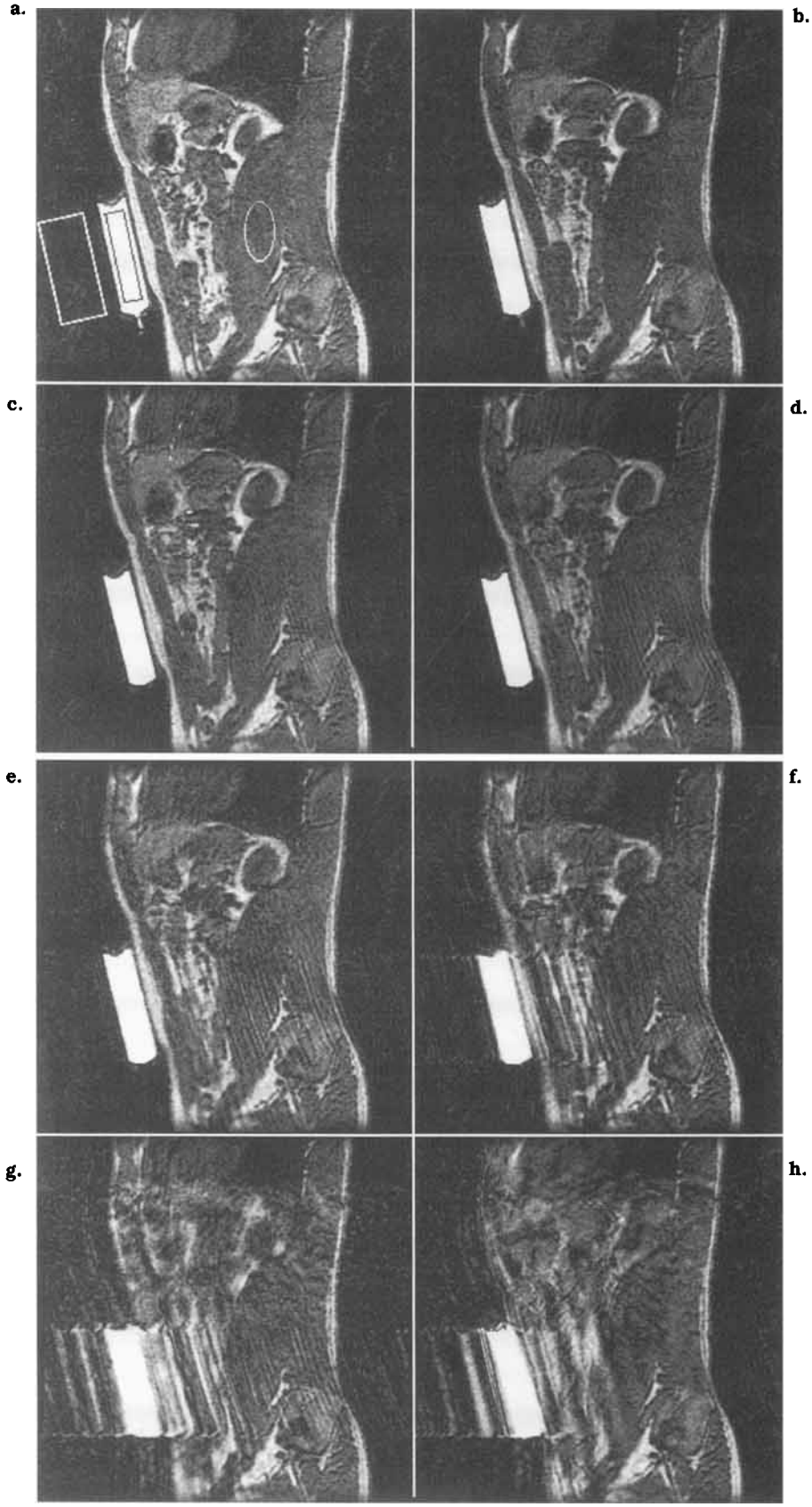

Figure 2. Representative sagittal 3D spoiled gradient-echo images (TR = 7 msec, TE = 1.2 msec, 32 slices, 3.5-mm slice thickness, flip angle = 30°, matrix = 256 × 192) through a Gd-filled phantom taped to the abdomen of a human volunteer. (**a**) Breath-hold, with representative ROIs for phantom, air, and psoas muscle; (**b**) 80% central breath-hold; (**c**) 65% central breath-hold; (**d**) 50% central breath-hold; (**e**) 35% central breath-hold; (**f**) 20% central breath-hold; (**g**) free breathing; (**h**) 75% peripheral breath-hold. All are displayed with the same window and level.

a. b. c.

Figure 3. MIP images from renal 3D Gd-MRA images of three different patients using different breathing algorithms: **(a)** free breathing, **(b)** 57% breath-hold during central k-space acquisition, **(c)** 100% breath-hold. Note that whereas the 57% breath-hold does have a perceptibly decreased SNR compared with a 100% breath-hold, the renal arteries and their branches remain quite sharp. In contrast, the free-breathing study is nondiagnostic.

breath-holding occurs relative to k-space acquisition (Figs. 1b and 1c). As anticipated, the amount of ghosting, blurring, and general image degradation is significantly less for a partial breath-hold occurring during acquisition of the central portion of k space (Fig. 4). As can be seen, there is an immediate, abrupt drop-off in SNR for peripheral breath-holding. For breath-hold fractions of less than 70% to 80%, these data show no benefit over free breathing. Central breath-holding, on the other hand, demonstrates a more gradual decline in SNR, with the large tube having a 22% decrease in SNR for a 65% breath-hold and a 28% SNR loss for a 50% breath-hold.

Examining modeled blur (Fig. 5), blur values remain at or below the 1-pixel threshold (2.1 mm for a 40-cm FOV) for central breath-holds down to 50%. Peripheral breath-holding data are not plotted, because blur rapidly increased with decreased breath-holding. For central breath-holds of less than 30%, some interesting effects are seen. Blur rapidly increases to a maximum at a 10% to 20% breath-hold (depending on phantom size), followed by decreased blur as breath holding approaches 0%. This seemingly paradoxic effect can be explained by the model. As would occur in a patient, breath-holding is modeled as full inspiration (maximum pixel displacement) followed by cyclical respiration after the breath-hold period ends. The cyclic respiration (modeled as a repeating Gaussian rather than a sinusoid — see Methods section) is such that the average position is much closer to zero than to maximum displacement. Therefore, for short (10%–20%) breath-holds, the central-most aspect of k space (during the breath-hold) is acquired with a constant maximum displacement, and the remainder (which still includes a region quite central in k space) has a cyclic phase shift that averages closer to zero. The net result of this discontinuity in phase shifts causes a more continuous distribution of the ghosting artifacts (compare Figs. 1e and 1f), resulting in a larger amount of blurring than in the free-breathing case. This effect is not seen if the breath-hold is modeled as full expiration followed by the same cyclic respiratory motion, because in this case, the difference between the average displacement during respiration and the displacement during central k-space acquisition is not as great.

The computer model also allows us to examine the effects of partial breath-holding on different-sized objects (Fig. 4). Note that the smallest phantom (6.25 mm) has decreased SNR compared with the larger phantoms (12.5 and 25 mm) at almost all breath-hold fractions but is most notably degraded for breath-holding less than 40%. This effect can be best explained by the fact that smaller objects have a relatively greater high spatial frequency content. This means that small objects are most perturbed by the respiratory-induced phase shifts that occur at smaller breath-hold fractions.

Figure 4 demonstrates another characteristic related to object size. Note that the "ripple" superimposed on the central breath-hold SNR measurements is inversely proportional to the vessel size. We believe that this effect occurs due to differences in k-space representation for the three objects. Because these simulated objects are essentially rect functions, their Fourier transform is a sinc function. The wider the object, the narrower the sinc function. Because of the way the model is implemented, individual respiratory excursions "propagate" through the collection of the peaks and nulls of the sinc function as the breath-hold fraction changes. Because perturbations occurring in the high signal portions of k space (peaks) have greater effect than those occurring in the lower signal portions of k space (nulls), a large object with a narrow Fourier representation (peaks and nulls of the sinc closer together) would be expected to have a higher frequency of "variability" in artifact than a small object with a broad Fourier representation. This is precisely what is seen in Figure 4. This observation is important, at least in theory, because it demonstrates the effects of a certain "randomness" in how the phase of respiratory motion happens to relate to the energy content of k space. Note, for instance, that in Figure 4 the SNR for the 25-mm object at a central breath-hold of 65% is actually better than for a breath-hold of 75%.

Human Imaging

As anticipated and predicted by the modeling study, respiratory artifact is dramatically less for partial breath-holds occurring in the central portion of k space (Figs. 2, 6, and 7). This is shown statistically in rows 1 through 3 of Table 1. There is, however, a statistically significant improvement in SNR for a mere 20% central breath-hold (Table 1, rows 4 and 5). This becomes significant for image blur at a 35% early breath-hold. Statistical analysis of differences in SNR between a complete breath-hold and varying amounts of central breath

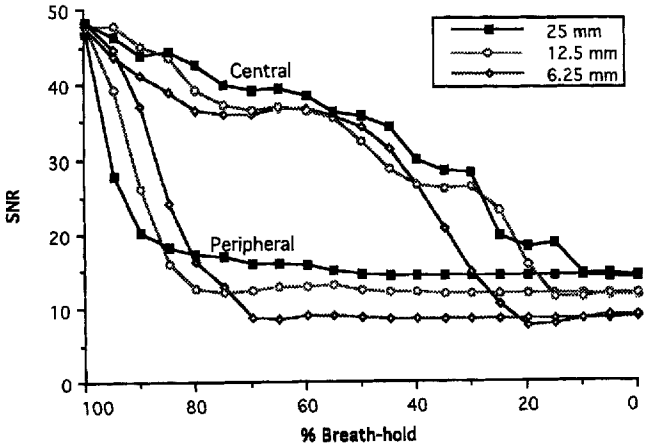

Figure 4. Simulated SNR versus breath-hold fraction for "vessel" diameters of 25, 12.5, and 6.25 mm. Modeled data for partial breath-holds coinciding with central and peripheral k-space acquisition.

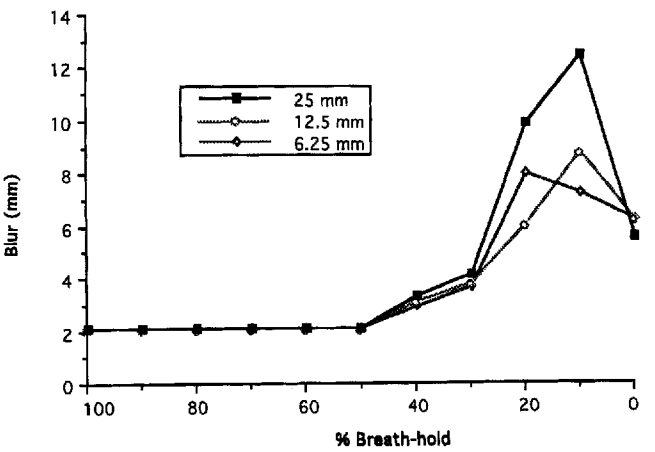

Figure 5. Simulated image blur versus breath-hold fraction for "vessel" diameters of 25, 12.5, and 6.25 mm. Modeled data for partial breath-holds coinciding with central k-space acquisition.

holding revealed high statistical significance at the first increment (difference between 100% and 80% breath-hold) for the phantom (Table 1, rows 6 through 9). Fat and liver SNR were not significantly different from a complete breath-hold until a 35% breath-hold fraction (although the significance for liver was marginal at 80%). Interestingly, central breath-hold phantom blur was not significantly different from a complete breath-hold until a fraction of 50%.

Therefore, although SNR for central breath-holding decreases in a statistically significant fashion as breath-hold fraction decreases (Fig. 6), edge blur remains relatively constant down to an approximately 50% central breath-hold (Fig. 7). From examining partial breath-hold images (Fig. 2), the loss in SNR seems to be mainly due to low amplitude, high frequency ghosting in the phase direction emanating from abrupt interfaces (ie, air-phantom). Examining Figure 6, there is the suggestion that SNR drops off more rapidly for central breath-holds less than 50% than it does for breath-holds greater than 50%. This is corroborated in the simulation images (Fig. 4). For the phantom, SNR loss for 50% central breath-holding is only 21%. For liver and fat, it is 6% and 11%. For a 65% breath-hold, these numbers drop to only 13%, 6%, and 6%, respectively. This means the SNR penalty for breath-holds of at least 50% is not too severe if the breath-holding occurs in the central portion of k space.

Comparing the central breath-hold images with the free breathing or peripheral breath-hold images, internal structure remains well defined despite the decrease in SNR, at least down to an approximately 50% breath-hold (Fig. 2). This is due to the relative plateau in edge blurring for early breath-holds of greater than 50%, as seen in Figure 7. Average blur only increases from 2.2 to 3.3 mm for a 50% breath-hold and to 2.5 mm for a 65% breath-hold. Therefore, only minimal loss of sharpness occurs for early partial breath-holds of 50% or greater.

Using a slightly different approach to evaluating image degradation, contamination can be defined for a given ROI as the increase in variance (square of the SD) due to motion. Contamination differs from SNR in that it reflects the change in pixel-to-pixel variability of a homogeneous structure (in this case, psoas muscle) caused by respiratory-induced artifacts without considering the mean signal of the ROI, which may itself be altered due to these artifacts. For the psoas muscle, contamination increased by 172% between a full breath-hold and full breathing. For 80%, 65%, and 50% central breath-holds, contamination values were approximately 3%, 17%, and 50%, respectively.

Modeled Versus Human Data

The human subject results are predicted by the computer model, as agreement between subject and modeled data is quite good, thus validating our computer model as a method of evaluating the effects of partial breath-holding (Figs. 6 and 7). This is especially true, considering the large amount of subject-to-subject variation in respiratory rate and amplitude, which makes precise modeling of the human data difficult. Because we measured an average phantom displacement (full inspiration/expiration) of 1.95 + .75 cm (AP) and .60 + .4 cm (SI) in our human volunteers, a value of approximately half of the AP excursion seemed appropriate considering the subjects were not breathing with maximal respiratory excursion. Therefore, for the modeling study, we chose a 4-pixel respiratory excursion, which for an FOV of 40 cm with 192 phase encodings, corresponds to an excursion of 8.3 mm.

Application to Gd-MRA

The insights gained through the simulation and volunteer patient images were applied to clinical Gd-MRA. Figures 3a through 3c demonstrates representative MIPs from three different patients who underwent routine renal Gd-MRA to rule out renal artery stenosis. In Figure 3a, in which the patient breathed freely, there is severe blurring and ghosting of the vasculature, with poor visualization of the renal arteries much beyond their origin. This study was deemed of inadequate quality for diagnostic purposes. Compare this to Figures 3b and 3c, which are similar studies, only with 57% and 100% breath-holds, respectively. Both were deemed adequate for clinical diagnosis. Note the definition of the distal renal arteries and proximal renal artery branches in both studies, without appreciable blurring. The only perceptible differences between the 100% breath-hold (Fig. 3c) and the 57% breath-hold (Fig. 3b) are a loss in definition of the tiny distal vessels and a mild increase in background noise for the 57% breath-hold.

• DISCUSSION

Rapid MRI of the abdomen and chest is increasingly performed during suspension of respiration to eliminate

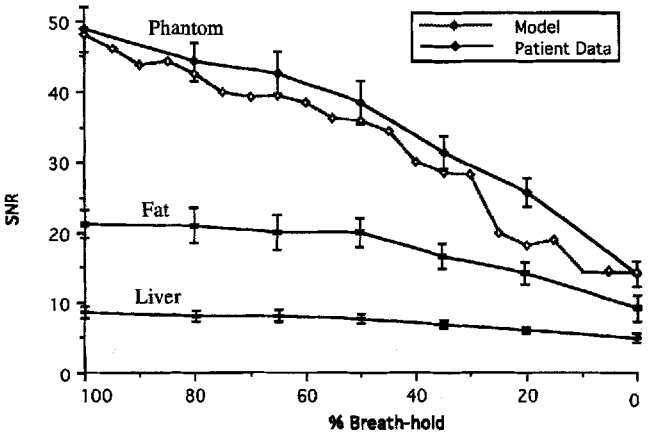

Figure 6. Averaged data for 10 human subjects showing SNR versus central breath-hold fraction for phantom, infrarenal perinephric fat, and liver (imaging parameters are the same as in Figure 2). Superimposed modeled data for a large (25-mm) "vessel."

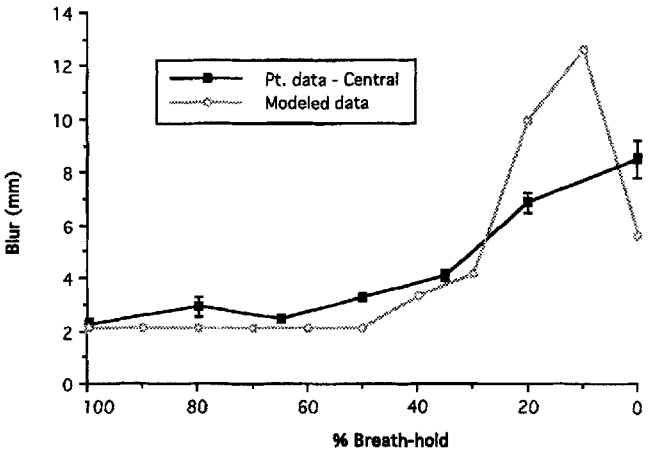

Figure 7. Averaged data for 10 human subjects showing blur (at anterior margin of phantom) versus breath-hold fraction. Data plotted for partial breath-holds coinciding with both central and peripheral k space. Superimposed modeled central breath-hold data for a large (25-mm) "vessel."

respiratory motion artifacts (10–14). Many patients, however, are not able to suspend breathing for the entire scan duration. Although many non-breath-hold techniques have been described to decrease respiratory artifacts, and many are used routinely, none are as effective as complete cessation of respiratory motion (1,3,6,15,16). When breath-holding fails, it is sometimes possible to repeat the study with a non-breath-hold technique. But breath-holding increasingly coincides with events that are difficult to repeat, such as a dynamic Gd bolus. In these instances, designing a scanning/breath-holding strategy that still works in the event of partial breath-holding is essential.

Optimum Breath-Holding Strategy

These computer simulation and imaging experiments in 10 subjects, as well as the clinical 3D Gd-MRA example, demonstrate that most benefit from breath-holding can be achieved by suspending respiration during central k-space acquisition. This is understandable considering that the central portion of k space contains the most signal energy and contributes most to gross image contrast (17). Breathing during this critical central portion of k space (Figs. 1c, 1f, and 3a) has devastating consequences on image quality such that no significant improvement in SNR or image blur is seen between free breathing and as much as a 75% peripheral breath-hold (Table 1). Therefore, imaging strategies in which respiratory motion may occur during acquisition of central k space must be avoided. By way of comparison, central breath-holds of 50% or more lead to only a mild reduction in SNR (on the order of 20% or less). Perhaps even more importantly, corresponding image blur increases only slightly over this breath-holding range (approximately 1 mm or less).

Although a full breath-hold is always preferred, partial breath-hold imaging may be unavoidable in many cases, as a-priori estimation of a patient's breath-hold capacity is difficult. Under circumstances in which image sharpness is of paramount importance (such as MRA), partial breath-holding may be the best that can be achieved, particularly if constrained by imager speed limitations and slice coverage/resolution requirements. Alternatively, one may question the consequences of intentionally pushing a patient beyond his breath-hold endurance. Given these considerations, an optimum breath-holding strategy requires that breath-holding should occur during the acquisition of central k space and then last as long as possible into the acquisition of peripheral k space. Centric phase encoding is well suited to this task (8,17–20). Using centric phase encoding, the patient is asked to begin a breath-hold just before the scan begins, while it is still easy to communicate. The patient is instructed to continue the breath-hold as long as possible or until the scan ends. When data acquisition begins, the center of k space is collected immediately. As time progresses, the more peripheral lines of k-space data are acquired. Whenever the patient begins breathing, maximum breath-hold duration and central position within k space are ensured. We have used the term "centric" to represent centric only in the slow phase-encode direction. Other more completely centric sequences, such as square spiral or elliptical spiral centric, can be devised and are even less sensitive to partial breath-holding artifacts (18–20).

The combination of partial breath-holding and centric phase encoding can be used with 3D Gd-MRA (Fig. 3). If bolus timing is determined by using a test dose or by monitoring the aorta for arrival of the arterial phase, centric phase encoding simultaneously provides optimal arterial enhancement and optimal breath-holding strategy (21,22). This occurs because the peak arterial contrast, initiation of breath-holding, and center of k space all coincide. The main drawback of centric encoding in combination with 3D Gd-MRA is that it is prone to ringing type artifacts caused by rapid changes in intravascular Gd concentration during central k-space acquisition (22).

Another important consideration in evaluating image degradation is object size. As demonstrated in Figure 4, modeled SNR for the smallest tube (6.25 mm) is generally less than that of the larger tubes and decreases sharply for breath-hold fractions less than 50%. This effect is also seen in Figure 3b, in which the tiny distal renal vessels are not optimally seen. This suggests that an approximately 50% breath-hold should stand as the minimum acceptable breath-hold fraction when high resolution is important (which it nearly always is). Of course, this determination will be left up to the individual radiologist based on the specific application and desired results. Using partial breath-holding in conjunction with Gd-MRA, in which it has been shown that the dynamic change in intra-arterial Gd concentration during data acquisition

Table 1
Statistical Significance of Changes in SNR and Blur for Different Partial Breath-Hold Algorithms Among 10 Volunteer Subjects

Breath-hold duration type	*P* value			
	Phantom SNR	Fat SNR	Liver SNR	Phantom Blur
25% peripheral versus 20% central	$3*10^{-3}$	$9*10^{-3}$	**.3**	**.8**
50% peripheral versus 50% central	$6*10^{-6}$	$3*10^{-5}$	$5*10^{-3}$	$2*10^{-3}$
Free breathing versus 75% peripheral	**.6**	**.3**	**.3**	**.1**
Free breathing versus 20% central	$5*10^{-5}$	$2*10^{-4}$	.01	**.1**
Free breathing versus 35% central	$5*10^{-6}$	$2*10^{-6}$	$6*10^{-4}$	$8*10^{-5}$
100% versus 80% central	$2*10^{-4}$	**.9**	.02	**.09**
100% versus 65% central	$2*10^{-3}$	**.1**	**.06**	**.2**
100% versus 50% central	$1*10^{-4}$	**.1**	.01	$4*10^{-6}$
100% versus 35% central	$1*10^{-4}$	$4*10^{-5}$	$2*10^{-3}$	$9*10^{-8}$

Note.—*P* values in **bold** are not statistically significant at the .05 level. Central breath-hold = during central k-space acquisition, peripheral breath-hold = during peripheral k-space acquisition.

leads to decreased signal in small vessels, these two effects are additive (22). This must be considered as attempts are made to image smaller vessels using Gd-MRA.

Breath-holding is simple to implement, is effective, and adds no imaging time. Unfortunately, many patients are limited in their breath-holding abilities. Based on the data presented here, however, even incomplete breath-holds have a significant capacity to decrease image blur and other respiratory artifacts, if the breath-hold occurs during central k-space acquisition and is of at least 50% duration. Although a full breath-hold is always preferred, this strategy, especially if combined with centric acquisition, allows one to push the patient's breath-holding abilities with only mild sacrifices in image quality if the patient cannot complete the entire breath-hold. As a final point, partial breath-holding has the potential to be used in conjunction with other respiratory artifact suppression techniques, such as respiratory gating, after breathing resumes.

References

1. Wood ML, Runge VM, Henkelman RM. Overcoming motion in abdominal MR imaging. Am J Roentgenol 1988; 150(3):513–522.
2. Haacke EM, Patrick JL. Reducing motion artifacts in two-dimensional Fourier transform imaging. Magn Reson Imaging 1986; 4(4):359–376.
3. Wood ML, Henkelman RM. Suppression of respiratory artifacts in magnetic resonance imaging. Med Phys 1986; 13(6):794–805.
4. Runge VM, Wood ML. Fast imaging and other motion artifact reduction schemes: a pictorial overview. Magn Reson Imaging 1988; 6(5):595–607.
5. Holland GA, Dougherty L, Carpenter JP, et al. Breath-hold ultrafast three-dimensional gadolinium-enhanced MR angiography of the aorta and the renal and other visceral abdominal arteries. Am J Roentgenol 1996; 166:971–981.
6. Ehman RL, Felmlee JP. Adaptive technique for high-definition MR imaging of moving structure. Radiology 1989; 173(1):255–263.
7. Holsinger AE, Riederer SJ. The importance of phase encoding order in ultra-short TR snapshot MR imaging. Magn Reson Med 1990; 16:481–488.
8. Jones RA, Rinck PA. Approach to equilibrium in snapshot imaging. Magn Reson Med 1990; 8:797–803.
9. Henkelman RM. Measurement of signal intensities in the presence of noise in MR images. Med Phys 1985; 12(2):232–233.
10. Prince MR, Narasimham DL, Stanley JC. Breath-hold gadolinium-enhanced angiography of the abdominal aorta and its major branches. Radiology 1995; 197:785–792.
11. Rydberg JN, Lomas JL, Coakley KJ, Hough DM, Ehman RL, Riederer SJ. Comparison of breath-hold fast spin-echo pulse sequences for T2-weighted MR imaging of liver lesions. Radiology 1995; 194:431–437.
12. Butts K, Riederer SJ, Ehman RL. The effect of respiration on the contrast and sharpness of liver lesions in MRI. Magn Reson Med 1995; 33(1):1–7.
13. Alsop DC, Hatabu H, Bonnet M, Listerud J, Gefter W. Multislice, breath-hold imaging of the lung with submillisecond echo times. Magn Reson Med 1995; 33(5):678–682.
14. Leung DA, McKinnon GC, Davis CP, Pfammatter T, Krestin GP, Debatin JF. Breath-hold, contrast-enhanced, three-dimensional MR angiography. Radiology 1996; 201:569–571.
15. Haacke EM, Lenz GW, Nelson AD. Pseudo-gating: elimination of periodic motion artifacts in magnetic resonance imaging without gating. Magn Reson Med 1987; 4:162–174.
16. Shetty AN, Shirkhoda A, Bis KG, Alcantata A. Contrast-enhanced three-dimensional MR angiography in a single breath-hold: a novel technique. Am J Roentgenol 1995; 165:1290–1292.
17. Riederer SJ, Tasciyan T, Farzaneh F, Lee JN, Wright RC, Herfkens RJ. MR fluoroscopy: technical feasibility. Magn Reson Med 1988; 8(1):1–15.
18. Wilman AH, Riederer SJ, Breen JF, Ehman RL. Elliptical spiral phase-encoding order: an optimal field-of-view-dependent ordering scheme for breath-hold contrast-enhanced 3D MR angiography. Radiology 1996; 201(P):328–329.
19. Bampton AEH, Riederer SJ, Korin HW. Centric phase-encoding order in three-dimensional MP-RAGE sequences: application to abdominal imaging. JMRI 1992; 2:327–334.
20. Korin HW, Riederer SJ, Bampton AEH, Ehman RL. Altered phase-encoding order for reduced sensitivity to motion in three-dimensional MR imaging. JMRI 1992; 2:687–693.
21. Foo TK, Manojkumar S, Prince MR, Chenevert TL. MR smart prep: an automated method for detecting the bolus arrival time of initiating data acquisition in fast 3D gadolinium-enhanced MRA (abstract). In: Proceedings of the 4th annual scientific meeting of the International Society for Magnetic Resonance in Medicine. New York: International Society for Magnetic Resonance in Medicine, 1996; 453.
22. Maki JH, Prince MR, Londy FJ, Chenevert TL. The effects of time varying intravascular signal intensity and k-space acquisition order on three-dimensional MR angiography image quality. JMRI 1996; 6:642–651.